# Effect of long-range hopping on dynamic quantum phase transitions of an exactly solvable free-fermion model: Nonanalyticities at almost all times

J. C. Xavier [1] and José A. Hoyos [2,3]

[1]*Universidade Federal de Uberlândia, Instituto de Física, C. P. 593, 38400-902 Uberlândia, Minas Gerais, Brazil*
[2]*Instituto de Física de São Carlos, Universidade de São Paulo, C. P. 369, São Carlos, São Paulo 13560-970, Brazil*
[3]*Max Planck Institute for the Physics of Complex Systems, Nöthnitzer Str. 38, 01187 Dresden, Germany*

In this work, we investigate quenches in a free-fermion chain with long-range hopping, which decay with the distance with an exponent $\nu$ and has range $D$. By exploring the exact solution of the model, we found that the dynamic free energy is nonanalytical in the thermodynamic limit, whenever the sudden quench crosses the equilibrium quantum critical point. We were able to determine the nonanalyticities of dynamic free energy $f(t)$ at some critical times $t^c$ by solving nonlinear equations. We also show that the Yang-Lee-Fisher (YLF) zeros cross the real-time axis at those critical times. We found that the number of nontrivial critical times, $N_s$, depends on $\nu$ and $D$. In particular, we show that for small $\nu$ and large $D$ the dynamic free energy presents nonanalyticities in any time interval $\Delta t \sim 1/D \ll 1$, i.e., there are nonanalyticities at almost all times. For the spacial case $\nu = 0$, we obtain the critical times in terms of a simple expression of the model parameters and also show that $f(t)$ is nonanalytical even for finite system under antiperiodic boundary condition, when we consider some special values of quench parameters. We also show that, generically, the first derivative of the dynamic free energy is discontinuous at the critical time instant when the YLF zeros are nondegenerate. On the other hand, when they become degenerate, all derivatives of $f(t)$ exist at the associated critical instant.

## I. INTRODUCTION

Equilibrium phase transitions (PTs) have been studied in detail and observed in several compounds in the last two centuries [1–3]. Along the lines (or planes, or points) that separate the distinct phases, the thermodynamic functions are nonanalytic. Due to this fact, the systems present unusual physical properties close to these lines. In general, we can not understand the phenomena close to the transition lines by a simple picture, such as the Fermi liquid for instance. For this reason, this subject has been of great interest for several physicist communities. The nonanalyticity of the thermodynamic functions is encoded in the zeros of the partition function $\mathcal{Z}$, the so-called Yang-Lee-Fisher (YLF) zeros [4–6]. In general, the zeros of $\mathcal{Z}(q) = \text{Tr}(e^{-qH})$ happen for $q = \beta + i\alpha$, where $\beta = \frac{1}{k_B T}$ and $\alpha \neq 0$. In the thermodynamic limit, however, these zeros can touch the real temperature axis yielding to nonanalyticities of the Helmholtz free energy $F = -k_B T \ln[\mathcal{Z}(\beta)]$. For a recent experimental verification of this phenomenon, see, for instance, Refs. [7,8]. A similar equilibrium partition function that is also studied is the boundary partition function $\mathcal{Z}^b(\beta) = \langle \psi^b | e^{-\beta H} | \psi^b \rangle$, i.e., the partition function ruled by the Hamiltonian $H$ with boundaries described by the boundary state $|\psi^b\rangle$ separated by $\beta$ [9–11].

In the last years [12–27], the concept of YLF zeros has been applied to sudden quenches: a parameter $\delta$ of a system Hamiltonian $H(\delta)$ changes from $\delta_0 \rightarrow \delta$ at the time instant $t = 0$. Specifically, the dynamical analog of the boundary partition function is the return probability $Z(t) = \langle \psi_0 | e^{-iH(\delta)t} | \psi_0 \rangle$, where $|\psi_0\rangle$ is the ground state of the Hamiltonian $H(\delta_0)$. The dynamical analog of the free energy is

$f(t) = -\frac{1}{N} \ln(|Z(t)|^2)$, where $N$ is the number of degrees of freedom, and can also be a nonanalytic function at some critical time $t^c$. For a review and generalizations to other out-of-equilibrium scenarios see, e.g., Ref. [28].

The quantum quench protocol we consider here is the following: the system is prepared in the ground state of $H(\delta_0)$ and then is time evolved according to $H(\delta)$, being $\delta$ some tuning parameter of $H$. The nonanalytical behavior of $f$ in time was called dynamical quantum phase transition (DQPT) [12] and was recently observed in experiments [20,23,25]. It is important to mention that, by now, it is well established that there is no one-to-one correspondence between DQPTs and equilibrium phase transitions [13,14,16–19,22].

Experimental observation of the DQPTs was observed recently [25], where trapped ions were used to simulate the transverse-field Ising chain with long-range interaction. The long-range interaction between two spins $i$ and $j$ is given by $J_{i,j} = \Omega^2 \nu_R \sum_m \frac{b_{im} b_{jm}}{\mu^2 - \nu_m^2}$ [29] and depends on the experimental setup, namely: the Rabi frequency $\Omega$ of the laser, the ion mass of the single ion via the recoil frequency $\nu_R$ associated with the dipole force, the orthonormal mode component of the $i$th ion $b_{im}$ with mode $m$ and frequency $\nu_m$, as well as the symmetric detuning $\mu$ of the beat note from the spin-flip transition [25,29–32]. It has been observed in trapped ion experiments that the long-range coupling $J_{i,j}$ can be approximated as $J_{i,j} \sim 1/|i - j|^\alpha$ where $0 < \alpha < 3$ depends on the laser detuning $\mu$ [25,29,33,34].

The effect of the long-range interactions in the context of the DQPTs were investigated in the transversal-Field Ising chain [18,19,24–26]. All those studies were done numerically

since the long-range interaction, in general, breaks integrability (exceptions exist and can be found in, e.g., Refs. [35,36]). Although numerical results can give strong evidence of the DQPTs, those methods are limited. In particular, the studies based on exact diagonalization and/or matrix product state (MPS) are limited by the size of the system, and/or by the bond dimension, as well as limited to short times. In principle and strictly according to the YLF zeros theory, the DQPTs manifest only in the thermodynamic limit. In this sense, a rigorous proof of the existence of a DQPT in the transversal-Field Ising chain with long-range interaction is still missing. In this vein, it is highly desirable to have a deep understanding of the long-range interaction effects in the context of DQPTs through analytical results. Insights into this issue may be gained by considering the free fermions with long-range hopping, since the model can be mapped, by using the Jordan-Wigner transformation, in a XX chain with long-range interaction. Although in this case, multiple spin interactions appear [37–39]. Very recently, the effect of the long-range hopping in the context of the DQPT were investigated in few models, like some variant of the Kitaev chain [40–42] (see also Refs. [35,36]). Motivated by the aforementioned facts, we investigate DQPTs in an exactly solvable free-fermion model with long-range hoppings.

The paper is organized as follows. In Sec. II, we present the model and its exact diagonalization. Analytical expressions for the dynamic free energy and the YLF zeros are determined in Sec. III together with numerical results. Our concluding remarks are given in Sec. IV.

## II. MODEL

We consider a free-fermion chain with long-range hoppings under twisted boundary condition given by the Hamiltonian

$$H(\delta) = \sum_{j=1}^{L} \frac{1+(-1)^j\delta}{2} \sum_{\ell=1}^{D} J_{j,2\ell-1}(c_j^\dagger c_{j+2\ell-1} + \text{H.c.}). \quad (1)$$

We consider systems of $L$ sites in which $L$ is even. The hopping amplitude decays as $J_{j,\ell} = J2^\nu(\ell+1)^{-\nu}$. Here, the constant $J$ sets the energy (or inverse time) unit of the system (and, from now on, is set to $J=1$), and $c_{j+L} = \exp(-\phi\pi i)c_j$ ($1 \leqslant j \leqslant L$), where $\phi$ defines the type of boundary condition: $\phi = 0$ means periodic boundary condition (PBC) and $\phi = 1$ means antiperiodic boundary condition (APBC). The exponent $\nu \geqslant 0$ controls the decay of the hopping amplitude with the distance, $D$ is the hopping range, and $\delta$ is the dimerization parameter, which tunes the system across an equilibrium quantum phase transition (QPT) at $\delta = 0$. For $D = 1$, this model recovers the dimerized chain with nearest-neighbor hopping, also known as Su-Schrieffer-Heeger (SSH) chain [43]. This model, for some particular choice of the parameters, was used to study symmetry-resolved entanglement entropy [39,44]. This is an interesting model because it allows one to investigate the effects of long-range hopping and is amenable to be solved by free-fermion techniques.

Note that the gauge transformation $c_j \to e^{-i\pi\Phi j/L}c_j$ makes the Hamiltonian translational invariant and, thus, can be diagonalized by the Fourier series. For the sake of completeness,

we present the main steps below. First, we introduce the new fermionic operators $\gamma_q$ and $\eta_q$ by

$$c_{2j} = \sqrt{\frac{2}{L}} \sum_q e^{2iqj}\eta_q, \text{ and } c_{2j-1} = \sqrt{\frac{2}{L}} \sum_q e^{iq(2j-1)}\gamma_q, \quad (2)$$

where the momenta are $q = q_n = \frac{2\pi}{aL}(n - \frac{\phi}{2})$, $n = 1, 2, \ldots, L/2$, and, from now on, we set the lattice spacing to $a = 1$. In terms of $\gamma_q$ and $\eta_q$ the Hamiltonian is

$$H = \sum_q (\gamma_q^\dagger \quad \eta_q^\dagger)\begin{pmatrix} 0 & C_q - i\delta S_q \\ C_q + i\delta S_q & 0 \end{pmatrix}\begin{pmatrix} \gamma_q \\ \eta_q \end{pmatrix},$$

$$= \sum_q \omega_{q,\delta}(\alpha_{+,q,\delta}^\dagger \alpha_{+,q,\delta} - \alpha_{-,q,\delta}^\dagger \alpha_{-,q,\delta}), \quad (3)$$

where

$$C_q = C_q(\nu, D) = \sum_{\ell=1}^{D} \ell^{-\nu} \cos[(2\ell-1)q], \quad (4)$$

$$S_q = S_q(\nu, D) = \sum_{\ell=1}^{D} \ell^{-\nu} \sin[(2\ell-1)q], \quad (5)$$

$$\omega_{q,\delta} = \omega_{q,\delta}(\nu, D) = \sqrt{C_q^2 + \delta^2 S_q^2}, \quad (6)$$

and

$$\alpha_{\pm,q,\delta} = \frac{1}{\sqrt{2}}(e^{i\theta_{q,\delta}}\gamma_q \pm e^{-i\theta_{q,\delta}}\eta_q) \quad (7)$$

are the eigenoperators associated to positive and negative branches of the dispersion relation $\pm\omega_{q,\delta}(\nu, D)$. Here, $\cos 2\theta_{q,\delta} = C_q/\omega_{q,\delta}$ and $\sin 2\theta_{q,\delta} = \delta S_q/\omega_{q,\delta}$.[1]

Finally, notice that

$$C_{\frac{\pi}{2}-q} = -C_{\frac{\pi}{2}+q}, \text{ and } S_{\frac{\pi}{2}-q} = S_{\frac{\pi}{2}+q}, \quad (8)$$

and that the ground state of $H(\delta)$ is

$$|\psi_0(\delta)\rangle = \prod_q \alpha_{-,q,\delta}^\dagger |0\rangle, \quad (9)$$

where the product is over all $q$'s in Eq. (2).

It is worth mentioning that for some special values of $\nu$ and $D$, the functions $C_q$ and $S_q$ can also be written in terms of some well-known functions, as depicted in Table I. For $\nu = \infty$ or $D = 1$, Eq. (6) recovers that of the nearest-neighbor hopping problem $\omega_{q,\delta} = \sqrt{\cos^2(q) + \delta^2 \sin^2(q)}$. The case $\nu = 0$ and $D = L/4$ is very peculiar and presents some anomalous characteristics (see Appendix). (i) The ground-state energy $E_0 \sim aL \ln L + bL$ is not extensive. (ii) Different boundary conditions lead to distinct behaviors. For PBC (APBC), the system is gapless (gapped) at half-filling. In addition, the difference $E_0^{\text{APBC}} - E_0^{\text{PBC}} \sim -L \ln L$.

---

[1]The quantities defined in Eqs. (4)–(7) depend on $q$, $\delta$, $\nu$, and $D$. To lighten the notation, only the dependence of $q$ and $\delta$ is kept in the subscript.

TABLE I. The functions $C_q(\nu, D)$ and $S_q(\nu, D)$ for some special values of $\nu$ and $D$. $\mathrm{Li}_\nu(z)$ is the polylogarithm function of order $\nu$.

| | $C_q(\nu, D)$ | $S_q(\nu, D)$ |
|---|---|---|
| $\nu = 0$ | $\frac{\sin(2Dq)}{2\sin q}$ | $\frac{1 - \cos(2Dq)}{2\sin(q)}$ |
| $\nu = 1$ $D = \infty$ | $-1/2[\cos(q)\ln(\lvert 2\sin q/2\rvert) - \sin(q)(\pi - 2q)]$ | $1/2[\cos(q)(\pi - 2q) + \sin(q)\ln(\lvert 2\sin q/2\rvert)]$ |
| $\nu = 2$ $D = \infty$ | $\frac{\pi^2}{6} - \frac{2q}{2} + \frac{q^2}{4}$ | $-\int_0^q \ln[2\sin(t/2)]dt$ |
| $\nu = \infty$ | $\cos(q)$ | $\sin(q)$ |
| $D = \infty$ | $\mathrm{Re}[e^{-iq}\mathrm{Li}_\nu(e^{i2q})]$ | $\mathrm{Im}[e^{-iq}\mathrm{Li}_\nu(e^{i2q})]$ |

## III. RESULTS

### A. Dynamic free energy and the YLF zeros

As we already mentioned, in our quench protocol the system is initialized in $|\psi_0(\delta_0)\rangle$, the ground state of $H(\delta_0)$, and time-evolved according to $H(\delta)$. Only $\delta$ is changed in the sudden quench, $\nu$ and $D$ remain constants. The return probability amplitude $Z(t) = \langle\psi_0(\delta_0)|e^{-iH(\delta)t}|\psi_0(\delta_0)\rangle$ can be evaluated following the same procedure of Refs. [27,45]. For completeness, we present below the main steps.

To time evolve $|\psi_0(\delta_0)\rangle$, we need the relation between the pre- and postquench eigenoperators $\alpha_{\pm,q,\delta_0}$ and $\alpha_{\pm,q,\delta}$ [see Eq. (3)]. This task is simple, since the wave numbers $q$ in (2), and, therefore, $\gamma_q$ and $\eta_q$, do not depend on $\delta$. Then, from Eq. (7), we find that

$$\alpha_{-,q,\delta_0}^\dagger = \cos(\Delta\theta_{q,\delta,\delta_0})\alpha_{-,q,\delta}^\dagger + i\sin(\Delta\theta_{q,\delta,\delta_0})\alpha_{+,q,\delta}^\dagger, \quad (10)$$

where $\Delta\theta_{q,\delta,\delta_0} = \theta_{q,\delta} - \theta_{q,\delta_0}$. Therefore,

$$Z(t) = \left\langle 0 \left| \prod_q \alpha_{-,q,\delta_0} e^{-iHt} \prod_k \alpha_{-,k,\delta_0}^\dagger \right| 0 \right\rangle$$
$$= \prod_q [\cos(\omega_{q,\delta}t) + ig_{q,\delta,\delta_0}\sin(\omega_{q,\delta}t)], \quad (11)$$

where $0 \leqslant g_{q,\delta,\delta_0} = \frac{C_q^2 + \delta\delta_0 S_q^2}{\omega_{q,\delta}\omega_{q,\delta_0}} \leqslant 1$.

Finally, the dynamic free energy $f(t) \equiv -L^{-1}\ln|Z(t)|^2$ is

$$f(t) = -\frac{1}{L}\sum_q \ln\left[\cos^2(\omega_{q,\delta}t) + g_{q,\delta,\delta_0}^2\sin^2(\omega_{q,\delta}t)\right], \quad (12)$$

and, in the thermodynamic limit, we can replace the sum by the integral

$$f(t) = -\int_0^{\pi/2} \frac{dq}{\pi} \ln\left[\cos^2(\omega_{q,\delta}t) + g_{q,\delta,\delta_0}^2\sin^2(\omega_{q,\delta}t)\right], \quad (13)$$

where the properties (8) were used to shorten the integration limit.

Let $\zeta_{n,m} = t_{n,m} + i\tau_n$ (or $\zeta_{q_n,m} = t_{q_n,m} + i\tau_{q_n}$) be the YLF zeros of $Z$. From Eq. (11), it is simple to show that

$$\zeta_{q_n,m} = \frac{(m - \frac{1}{2})\pi + \frac{i}{2}\ln\left(\frac{1 + g_{q_n,\delta,\delta_0}}{1 - g_{q_n,\delta,\delta_0}}\right)}{\omega_{q_n,\delta}}, \quad (14)$$

were $m \in \mathbb{N}_+$ is the $m$th accumulation line of YLF zeros, and $n = 1, \ldots, \frac{L}{2}$ labels the $n$th wave number $q_n$ in (2). Although there are $\frac{L}{2}$ YLF zeros per accumulation line, not all of them

are distinct because of (8). For $\frac{L}{2}$ odd, there are $\frac{1}{2}(\frac{L}{2} - 1)$ distinct zeros (which are doubly degenerated), and one (for $q = \pi$ for PBC and $q = \frac{\pi}{2}$ for APBC) has $|\tau_{q_n}| = \infty$. Thus, effectively there are $\frac{1}{2}(\frac{L}{2} - 1)$ zeros. For PBC and $\frac{L}{2}$ even, there are $\frac{1}{2}(\frac{L}{2} - 2)$ distinct zeros (which are doubly degenerated), and two zeros (for $q = \frac{\pi}{2}$ and $\pi$) with $|\tau_{q_n}| = \infty$. For APBC and $\frac{L}{2}$ even, there are $\frac{L}{4}$ doubly degenerated distinct zeros.

The DQPTs occur whenever $\tau_{q_n} = 0$ and, thus, from Eq. (14), they can only happen if $C_{q^c}^2 + \delta\delta_0 S_{q^c}^2 = 0$, i.e.,

$$T_{q^c}^2(\nu, D) \equiv \frac{S_{q^c}^2(\nu, D)}{C_{q^c}^2(\nu, D)} = -\frac{1}{\delta\delta_0}. \quad (15)$$

Notice the necessary condition $\delta\delta_0 < 0$, which corresponds to the quench crossing the equilibrium QPT of the model at $\delta_{\mathrm{eq}}^c = 0$.[2] Once the set $\{q^c\}$ is determined from Eq. (15), the time instants of the DQPTs are simply $t_{\{q^c\},m}^c = \frac{(2m-1)\pi}{2\omega_{q^c,\delta}}$. Due to the properties (8), if $q^c$ is a solution of (15), so is $\pi - q^c$. In addition, they provide the same YLF zero since $\omega_{q,\delta} = \omega_{\pi-q,\delta}$. Thus, it is sufficient to consider only the values of $q$ in the domain $[0, \frac{\pi}{2}]$ when solving for $\{q^c\}$ in (15).

In general, Eq. (15) admits no solution for finite systems since $\{q_n\}$ in Eq. (2) is a discrete set. Nonetheless, as reported in Appendix, for some special values of $\nu$, $D$, $\delta$, and $\delta_0$, Eq. (15) admits solutions for finite systems and, thus, for a real-time instant $t^c$, $f(t^c)$ is nonanalytic even for finite $L$. Nonanalyticities in finite-size systems were also reported in Refs. [13,15].

### B. Case of nearest-neighbor ($D = 1$) and third-nearest-neighbor ($D = 2$) hoppings

For completeness, we now briefly review the results for $D = 1$ and compare them with the case $D = 2$. It turns out that this comparison is very instructive to understand the case of generic $D$.

For $D = 1$ and $\delta\delta_0 < 0$, Eq. (15) gives a single solution $q^c = \arctan(\frac{1}{\sqrt{-\delta\delta_0}}) \in [0, \frac{\pi}{2}]$ [see Fig. 1(a)]. This means that each accumulation line in (14) provides only one real-time instant $t_{q^c,m} = (m - \frac{1}{2})\pi\sqrt{\frac{1 - \delta\delta_0}{\delta(\delta - \delta_0)}}$ in which the dynamic free energy is nonanalytic in the thermodynamic limit [see

---

[2]$\delta_{\mathrm{eq}}^c$ is determined by requiring $\omega_{q^c} = 0$ in Eq. (6). For $\nu \neq 0$, $S_q(\nu, D) \neq 0 \,\forall q$, and thus, $\delta_{\mathrm{eq}}^c = 0$. Notice it does not depend on $\nu$, which is quite different from the transverse-field Ising model with long-range interaction [18].
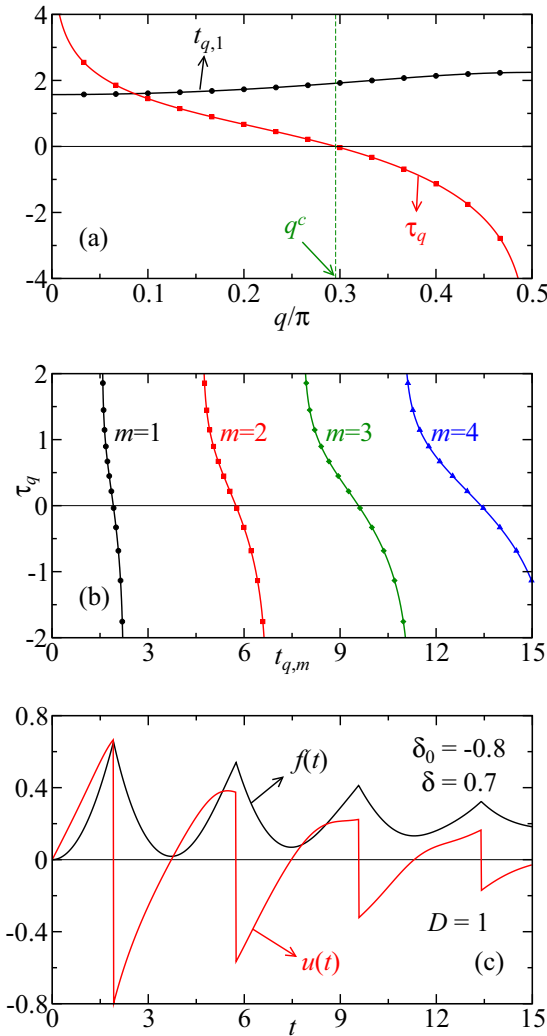
FIG. 1. In (a) and (b) we show the Yang-Lee-Fisher zeros $\zeta_{q_n,m}$ [Eq. (14)] for $D = 1$. (a) $t_{q,1}$ and $\tau_q$ as a function of the momentum $q$ (for accumulation line $m = 1$). (b) The complex-time plane (for $m = 1, \ldots, 4$). (c) The associated dynamical free energy $f$ [Eq. (13)] and its time derivative $u$ as a function of $t$. In (a), $q^c$ denotes the momentum associated with the real-time YLF zero. The symbols in (a) and (b) correspond to the allowed values of $q$ for a finite chain of length $L = 60$. The continuous lines in (a), (b), and (c) correspond to the thermodynamic limit. The sudden quench is from $\delta_0 = -0.8$ to $\delta = 0.7$.

Fig. 1(b)]. This nonanalyticity is manifest as a cusp in $f(t)$ (or a discontinuity in the dynamic internal energy $u \equiv \frac{\partial f}{\partial t}$) at $t = \zeta_{q^c,m} = t_{q^c,m}$ [see Fig. 1(c)]. Note that for the case $D = 1$, the results do not depend on the value of $\nu$.

Precisely, the nonanalyticity of the dynamic free energy can be quantified by analyzing the behavior of the YLF zeros near the real-time axis. From the Weierstrass factorization theorem [4–6], the singular part of the free energy due to the zero in the $m$th accumulation line is $f_{\text{n-a}} = -L^{-1} \sum_n \ln(\zeta - \zeta_{q_n,m}) + \text{c.c.}$. Here, c.c. stands for complex conjugate and accounts for the zeros of $\bar{Z}$ (the complex conjugate of $Z$). In the thermodynamic limit, $\zeta_{q_n,m}$ in Eq. (14) can be expanded near $q^c$ [see Fig. 1(a)]. Then, the real-time nonanalyticity of

the dynamic internal energy is quantified by

$$u_{\text{n-a}} = -\frac{1}{\pi} \int_{-\delta q}^{\delta q} \frac{d\tilde{q}}{\Delta t - (A_{q^c,m} - iB_{q^c})\tilde{q}} + \text{c.c.}, \quad (16)$$

where $\Delta t = t - \zeta_{q^c,m} = t - t_{q^c,m}$, $\tilde{q} = q - q^c$, $A_{q^c,m} = \frac{\partial t_{q,m}}{\partial q}|_{q=q^c} = -\frac{\delta_0(1-\delta^2)}{(\delta-\delta_0)\sqrt{-\delta\delta_0}} t_{q^c,m}$, $B_{q^c} = -\frac{\partial \tau_q}{\partial q}|_{q=q^c} = 2|\delta|\omega_{q^c,\delta}^{-3}$, and $\delta q$ is a positive constant whose value is unimportant for quantifying the nonanalyticity of $u$. The numerical prefactor is $\pi^{-1}$ and not $(2\pi)^{-1}$ because we are using the properties (8) to take into account the other YLF zero in the interval $q \in [\frac{\pi}{2}, \pi]$. By a simple integration (via residues, for instance), we can show that first derivative of the dynamic free energy has a discontinuity given by

$$\Delta u(\zeta = \zeta_{q,m}) = \lim_{\Delta t \to 0^+} u_{\text{n-a}} - \lim_{\Delta t \to 0^-} u_{\text{n-a}} = -\frac{4B_{q^c}}{A_{q^c,m}^2 + B_{q^c}^2}. \quad (17)$$

This is because the pole at $\tilde{q} = \frac{\Delta t}{A_{q^c,m} - iB_{q^c}}$ crosses the real-$\tilde{q}$ axis when $\Delta t$ changes sign. We have confirmed this result via numerical integration of (13).

For $D = 2$ and $\delta\delta_0 < 0$, the situation is more involved. If $\nu < \log_2 3 \approx 1.585$, Eq. (15) admits two additional solutions if $-\frac{1}{\delta\delta_0} > T_{q_{\min}}^2(\nu, D) = (\frac{3+2^\nu}{3-2^\nu})^3(\frac{2^\nu+1}{2^\nu-1})$ [see Fig. 2(a)]. This is because $T_q^2(\nu, D)$ has a local minimum at $q_{\min} = \frac{1}{2}\arccos(-\frac{4^\nu+3}{2^{2+\nu}})$. Thus, each accumulation line of YLF zeros crosses the real-time axis at three different instants [see Fig. 2(b)]. The corresponding density of YLF zeros crossing the real-time axis is a constant. Hence, as in the case $D = 1$, the corresponding nonanalyticities are cusps in $f(t)$ at those time instants [see Figs. 2(c) and 2(d)].

However, it is not straightforward to anticipate the resulting singularity when the two additional YLF zeros become degenerate, i.e., when $-\frac{1}{\delta\delta_0} = T_{q_{\min}}^2(\nu, D)$. Following the same steps as in Eq. (16), the singular part of the dynamical internal energy around the time instant $\zeta_{q_{\min},m} = t_{q_{\min},m}^*$ is

$$u_{\text{n-a}} = -\frac{1}{\pi} \int_{-\delta q}^{\delta q} \frac{d\tilde{q}}{\Delta t - (A_{q_{\min},m}\tilde{q} - \frac{i}{2}C_{q_{\min}}\tilde{q}^2)} + \text{c.c.}, \quad (18)$$

where $\Delta t = t - \zeta_{q_{\min},m} = t - t_{q_{\min},m}^*$, $\tilde{q} = q - q_{\min}$, $A_{q_{\min},m} = \frac{\partial t_{q,m}}{\partial q}|_{q=q_{\min}}$, $C_{q_{\min}} = -\frac{\partial^2 \tau_q}{\partial q^2}|_{q=q_{\min}}$, and $\delta q$, as before, is an unimportant positive constant. As for the case $D = 1$, the nonanalytical behavior of $u_{\text{n-a}}$ comes when a pole crosses the real-$\tilde{q}$ axis. However, we now face the situation where the integrand of $u_{\text{n-a}}$ has two poles. It is easy to see that one of the poles always remains far from the real-$\tilde{q}$ axis and, thus, does not contribute to the nonanalyticity. The other one does not cross the real-$\tilde{q}$ axis either. It only touches it when $\Delta t = 0$. As a result, the limit $u_{\text{n-a}}(t)$ as $t \to t_{q_{\min}}$ exists, i.e., $\Delta u = \lim_{\Delta t \to 0^+} u_{\text{n-a}} - \lim_{\Delta t \to 0^-} u_{\text{n-a}} = 0$. The same reasoning applies to all derivatives of $u$. Finally, we conclude that although $f$ is nonanalytic at $t_{q_{\min}}$, it is a smooth function (all derivatives exist) at that time instant [see Fig. 2(d)]. Nonetheless, we recall that this nonanalyticity poses a numerical challenge in computing $f$ and its derivatives at that time instant.

In analogy to the Ehrenfest's classification of the order of the equilibrium phase transitions [46], we could classify the order of the DQPTs by the lowest derivative of the dynamic
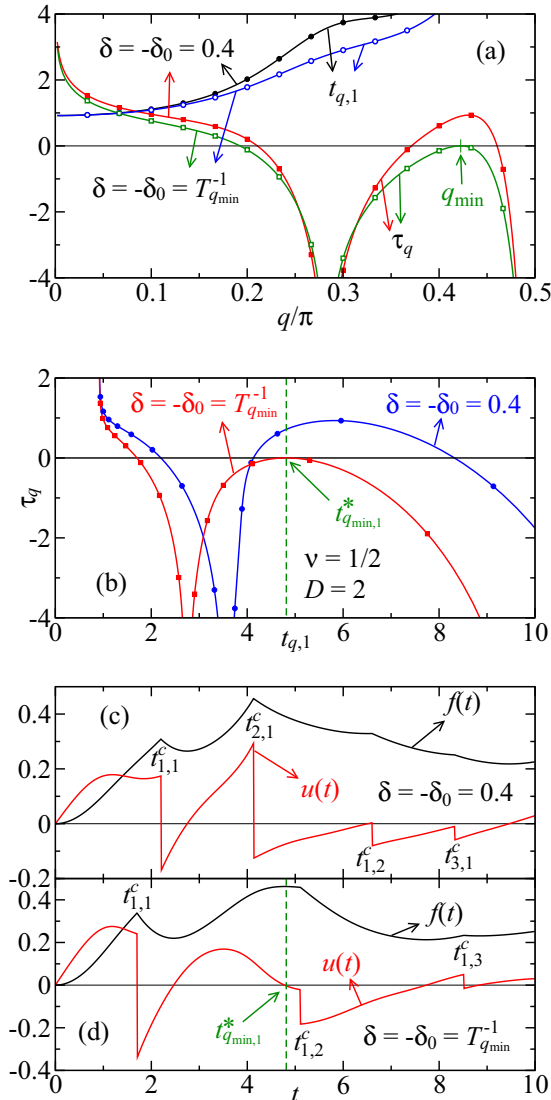
FIG. 2. In (a) and (b) we show the Yang-Lee-Fisher zeros $\zeta_{q_n,m}$ [Eq. (14)] for $D = 2$ and $\nu = 1/2$. (a) $t_{q,1}$ and $\tau_q$ as a function of the momentum $q$ (for accumulation line $m = 1$) and (b) in the complex-time plane (for $m = 1$). (c) and (d) The associated dynamical free energy $f$ [Eq. (13)] and its time derivative $u$ as a function of $t$. We consider two sudden quenches: (c) from $\delta_0 = -0.4$ to $\delta = 0.4$ (fulfilling $-\frac{1}{\delta\delta_0} > T^2_{q_{\min}}$) and (d) from $\delta_0 = -T^{-1}_{q_{\min}}(\nu, D)$ to $\delta = T^{-1}_{q_{\min}}(\nu, D) \approx 0.52$ (see legends). In (a), $q_{\min}$ denotes the momentum associated with the real-time YLF zero, which only touches the real-time axis. In (b) and (d), the corresponding time instant $t_{q_{\min}}$ is highlighted. The symbols in (a) and (b) correspond to the allowed values of $q$ for a finite chain of length $L = 60$. The continuous lines in (a), (b), (c), and (d) correspond to the thermodynamic limit.

free energy that is discontinuous at the transition. With this classification in mind, we observe that when the YLF zeros are not degenerate, the DQPT is of first order. On the other hand, when the YLF zeros become degenerate, the DQPT is of infinite order. It is then tempting to state that this is the dynamic analog of the Berezinskii-Kosterlitz–Thouless (BKT) transition of equilibrium systems. However, BKT transition has a continuous of YLF zeros in one of the phases. Here,
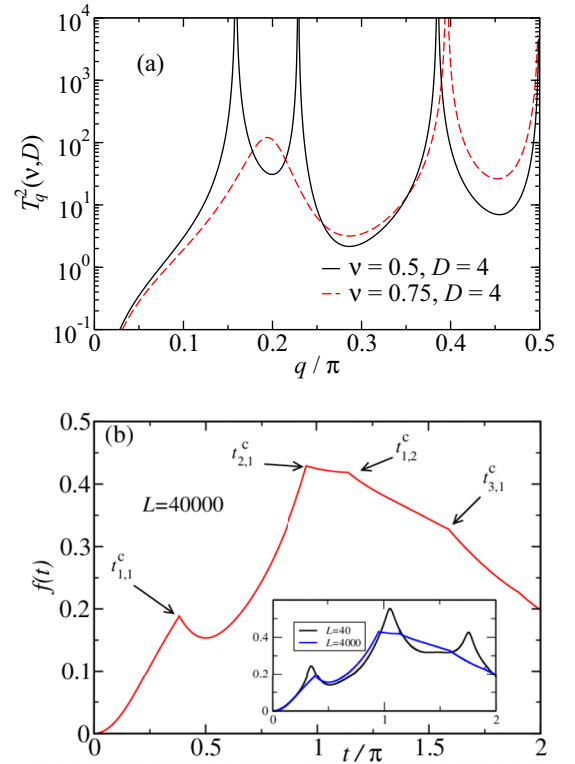


FIG. 3. (a) $T^2_{\nu,D}$ vs. $q$ for $D = 4$ and $\nu = 0.5$ and 0.75. (b) The dynamic free energy $f(t)$ vs. $t$ for a system of size $L = 40\,000$, $D = 4$, $\nu = 0.5$, and $\delta_0 = -\delta = 0.5$ [meaning Eq. (15) has three solutions for $0 < q < \frac{\pi}{2}$]. The arrows indicate the cusp positions, which are located at $t^c_{k,m}$ (see text). Inset: $f(t)$ for $L = 40$ and $L = 4000$.

there is no continuous distribution of YLF zeros after or before the instant of nonanalyticity $t^*_{q_{\min},m}$.

## C. Numerical results

As we show below, this feature of two dynamical QPTs becoming degenerate (either by fine tuning $\delta\delta_0$ or $\nu$) and the associated cusps annihilating each other is a general feature for all other values of the hopping range $D$.

We plot in Fig. 3(a) $T^2_q(\nu, D) \equiv \frac{S^2_q(\nu,D)}{C^2_q(\nu,D)}$ [see Eqs. (4) and (5)] for $\nu = 0.5$ and $D = 4$. Notice that $T^2_{\nu,D}$ diverges for $q$'s such that $C_q(\nu, D) = 0$. When $\nu$ is sufficiently small, $T^2_{\nu,D}$ has $D - 1$ local minima in the domain $q \in [0, \frac{\pi}{2}]$. This means that, for sufficiently large $-\frac{1}{\delta\delta_0}$, there are $2D - 1$ solutions of Eq. (15). Let $\{q^c_k\}$ be the set of solutions of Eq. (15) for generic values $-\frac{1}{\delta\delta_0} > 0$. Then, $k$ runs from 1 to $N_s$, where $1 \leqslant N_s \leqslant 2D - 1$. The corresponding critical times are $t^c_{k,m} = \frac{(2m-1)\pi}{2\omega_{q^c_k,\delta}}$. As a representative example, we plot in Fig. 3(b) $f(t)$ for $\delta_0 = -\delta = 0.5$ and $L = 40\,000$. For these parameters, we have that $N_s = 3$ with $t^c_{1,1} \approx 0.380\pi$, $t^c_{1,2} \approx 0.954\pi$, $t^c_{1,3} \approx 1.591\pi$, and $t^c_{2,1} \approx 1.141\pi$. The corresponding nonanalyticities are cusps. Evidently, these cusps become rounded for finite systems [see, for instance, the inset of Fig. 3(b)]. However, for the case $\nu = 0$, nonanalyticities occur even for finite systems (see Appendix).

As previously argued, the number of minima in $T_q^2$ is $D-1$ for sufficiently small $\nu$, yielding up to $N_s = 2D - 1$ solutions of Eq. (15) (critical time instants per accumulation line). This number has to diminish when $\nu$ increases as $N_s = 1$ for $\nu \to \infty$. This is clearly demonstrated in Fig. 3(a) for $\nu = 0.75$. Notice that, instead of only local minima, $T_q^2$ develops local maxima for larger values of $\nu$. This means that the number of critical time instants $N_s$ per accumulation line (solutions) is a nonmonotonic function of the quench parameters $\delta$ and $\delta_0$. This nontrivial behavior is demonstrated in Figs. 4(a) and 4(b) where we plot $N_s$ as a function of $\nu$ and $\delta$ for fixed $\delta_0 = 1$ and $D = 4$ and 40. Notice that $N_s$ always changes by $\pm 2$ as these solutions always appear or disappear in pairs. At the transition lines, two solutions degenerate. The resulting nonanaliticity is a smooth one as demonstrated for the case $D = 2$.

Having discussed the cases of large and small $\nu$, and small $D$, we now discuss the interesting case of small $\nu$ and $D \gg 1$. As we have argued there can be $2D - 1$ solutions of Eq. (15). This means the existence of many critical time instants per accumulation line. More interesting, it can be demonstrated that the largest critical time instant is of order unity and the smallest one is of order $D^{-1}$ [see Fig. 4(d)]. As shown in Fig. 4(c), these time instants are somewhat evenly distributed in the interval $[\sim D^{-1}, \sim 1]$ (see more details in Appendix). Intriguingly, this means that for large values of $D$ the dynamic free energy $f(t)$ will present a large number of nonanalyticities in time. This is not only because the number of critical time instants is of order $D$ per accumulation line. As many of those instants happen at $t^c \sim D^{-1}$, they reappear yet at short timescales in the other accumulation lines. As a result, $f(t)$ has nonanalyticities at almost all times if the quantum quench crosses the transition, $D$ is sufficiently large, and $\nu$ is sufficiently small (see Fig. 5).

## IV. FURTHER DISCUSSIONS AND CONCLUSIONS

We studied the dynamic free energy $f(t)$ of a free-fermion chain with long-range hopping couplings, which is described by Eq. (1), focusing on its nonanalyticities and the associated Yang-Lee-Fisher zeros.

For effective short-range hoppings (small $D$ or large $\nu$) the YLF zeros cross the real-time axis only in a few instants per accumulation line. In contrast, when the hoppings are sufficiently long ranged (large $D$ and small $\nu$), the number of times the YLF zeros cross the real-time axis increases with $D$ and are more or less evenly spread in the short time interval $0 < Jt \lesssim 1$, where $J$ is the microscopic energy scale.

We point out that these many nonanalyticities are different from other cases studied in the literature, where the YLF zeros accumulate in an area on the complex-time plane. This is the case for the Kitaev honeycomb model [47] and for disordered systems exhibiting dynamical Griffiths singularities [27]. In the thermodynamic limit, the infinitely many zeros crossing the real-time axis yield to nonanalyticities only at the edges of those distributions of zeros. Here, for the model Hamiltonian (1), the zeros do not become continuously distributed over an area on the complex-time plane. They remain distributed in lines that cross the real-time axis in many different time instants. Evidently, when the distance between these
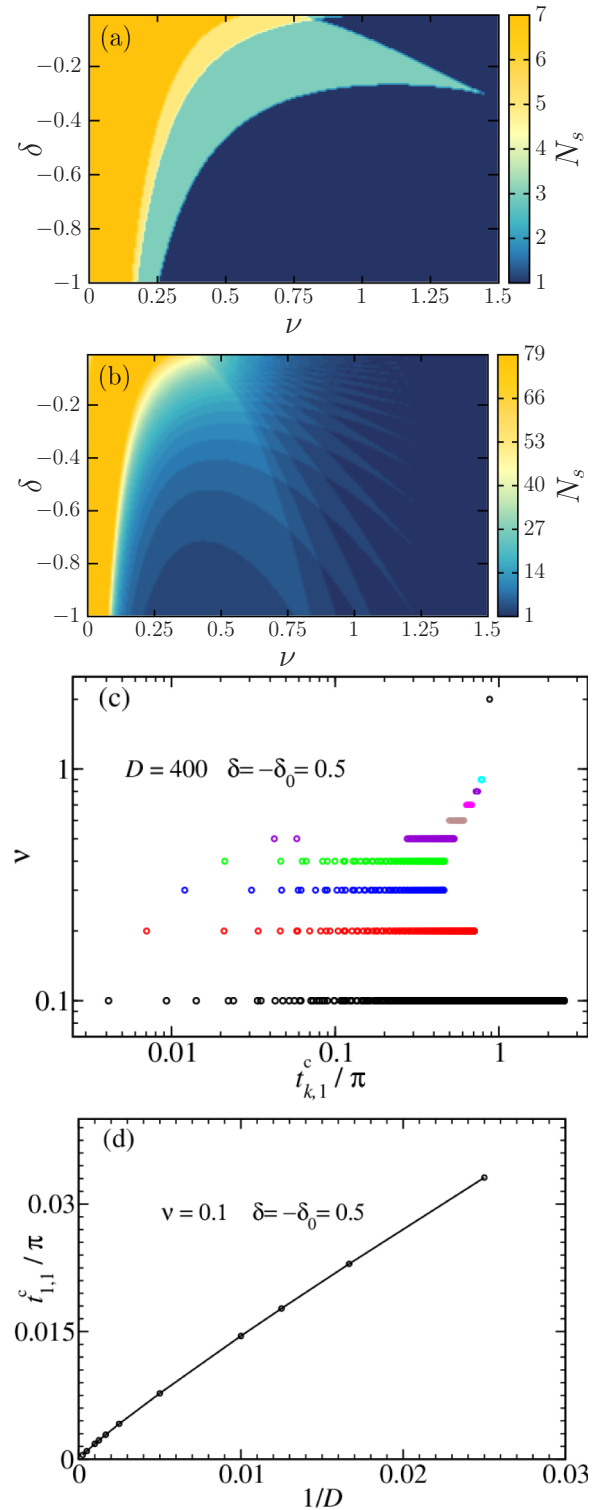


FIG. 4. (a) The number of solutions of Eq. (15), $N_s$, as a function of $\nu$ and $\delta$ for fixed $\delta_0 = 1$ and (a) $D = 4$ and (b) $D = 40$. (c) The critical times $t_{k,1}^c$ for various values of $\nu$, $D = 400$ and $\delta_0 = -\delta = 0.5$. (d) The earliest critical instant $t_{1,1}^c$ vs. $1/D$ for $\nu = 0.1$ and $\delta_0 = -\delta = 0.5$.

singularities increases beyond numerical or experimental resolution, they will appear as a smooth function of time, resembling the case of continuously distributed zeros over a time window.
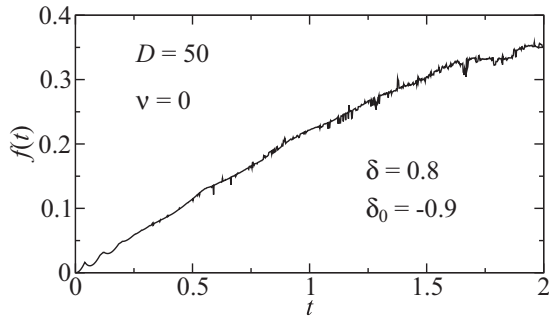
FIG. 5. The dynamical free energy $f$ as a function of time $t$ in the case $D = 50$ and $\nu = 0$ for the quantum quench from $\delta_0 = -0.9$ to $\delta = 0.8$. Many nonanalyticities appear already at short time scales.

We emphasize that the singularities are prominent only in sufficiently large systems (rigorously, only in the thermodynamic limit), especially when $D$ is large and $\nu$ small. Therefore, the observation of these many singularities in the current cold-atom platform, where the system size is not too large, may be a challenging task. Perhaps, the best way to circumvent this obstacle is to consider model with antiperiodic boundary condition, $D = L/4$, and $\nu = 0$ (see Appendix). For this situation, the YLF zeros lie on the real-time axis even for finite systems. We note that antiperiodic boundary conditions can be realized by considering the one-dimensional chain with periodic boundary condition with a magnetic field passing through the ring. For a particular choice of the flux magnetic, it is possible to map this model to one with the antiperiodic boundary condition (see, for instance, Refs. [48–50]).

To the best of our knowledge, long-range interaction effects in the context of DQPTs have only been studied for the transverse-Field Ising chain [18,19,24–26]. Although the model studied here is different, the present work may shed light on what happens in other models. For instance, in the transverse-field Ising model anomalous cusps (associated with the emergence of new cusps) in the dynamic free energy were reported when $\nu \lesssim 2.2$, at least for some quench parameters [18]. These cusps were denominated as anomalous simply because they are not equally spaced in time. As we have explicitly shown, new cusps not evenly separated in time appear for sufficiently long-range hopping (small $\nu$) in a nontrivial fashion (see Fig. 4) as predicted by Eq. (15). It is then desirable to understand Eq. (15) in a more fundamental way and/or generalize it to other systems, in particular, to nonintegrable ones. To this end, we recast Eq. (15) is terms of general quantities and find that it is equivalent to $\delta_0 \omega_{q,\delta}^2 + \delta \omega_{q,\delta_0}^2 = 0$. Thus, in the lack of a better analogy, the number of YLF zeros (or cusps) equals the number of Fermi point pairs of this weighted dispersion with zero chemical potential. While this is a simple fact for the model we studied, it would be desirable to verify it to other models. For the conventional nearest-neighbor transverse-field Ising chain, the analogous relation can be obtained by recasting the results of Ref. [12]: it is simply $\omega_{q,g}^2 + \omega_{q,g_0}^2 = (g - g_0)^2$, where the dispersion relation is $\omega_{q,g} = \sqrt{(g - \cos q)^2 + \sin^2 q}$ and $g = h/J$ is the ratio between the transverse field and the ferromagnetic coupling. Again, one needs to find the Fermi points of a weighted dispersion with chemical potential $(g - g_0)^2$. We emphasize that, in both models, the YLF zeros are determined uniquely by the knowledge of the dispersion relation and of the pre- and postquench parameters. It certainly desirable to verify whether this remains true for other models.

Finally, we mention that smaller the value of $\nu$, harder is the detection of the nonanalyticities numerically. In particular, the cusps become rounded if the system size is not sufficiently large [see Fig. 3] precluding its detection with exact diagonalization. On the other hand, powerful numerical techniques such as the tDMRG or the MPS use, typically, a time step $\Delta t \sim 0.01/J$ to evolve the initial state. Our results indicate that such time step is not sufficiently small to detect the nonanalyticities that appear already at short time scales when $1/(DJ) < 0.01/J$ (or $D \gtrsim 100$).

## APPENDIX: CASE $\nu = 0$

In this Appendix, we consider the special case that $\nu = 0$, where Eqs. (4) and (5) become

$$C_q = \frac{\sin(Dq)\cos(Dq)}{\sin q} \quad \text{and} \quad S_q = \frac{\sin^2(Dq)}{\sin q}. \quad \text{(A1)}$$

### 1. Critical time instants

We need to solve Eq. (15) with the care of having $\omega_q \neq 0$. Thus, we need to solve

$$\cos^2(Dq^c) + \delta_0 \delta \sin^2(Dq^c) = 0. \quad \text{(A2)}$$

As we are interested in solutions in the interval $q \in [0, \frac{\pi}{2}]$, then,

$$q_k^c = \frac{1}{D}\left[(k-1)\pi + \arcsin\left(\frac{1}{\sqrt{1 - \delta\delta_0}}\right)\right], \quad k = 1, \ldots, \frac{D}{2}. \quad \text{(A3)}$$

As we already mentioned in Sec. III, to solve Eq. (A2) we need that $D \ll L$, otherwise, there are not enough q's to satisfy this equation. Once we determine critical values of $q$ that satisfy Eq. (A2) we obtain the critical times $t_{i,n}^c = \frac{(2n-1)\pi}{2\omega_{q_i^c}(\delta)}$, $n = 1, 2, \ldots$, which are given by

$$t_{k,m}^c = \left(m - \frac{1}{2}\right)\pi \frac{1 - \delta\delta_0}{\sqrt{\delta(\delta - \delta_0)}} \sin(q_k^c). \quad \text{(A4)}$$

#### a. Limit $D \gg 1$

In this limit, the first critical instants ($k \ll D$) of each accumulation line $m$ become

$$t_{k,m}^c \approx \left(m - \frac{1}{2}\right)\pi \frac{1 - \delta\delta_0}{\sqrt{\delta(\delta - \delta_0)}}$$
$$\times \left(\frac{(k-1)\pi + \arcsin\left(\frac{1}{\sqrt{1 - \delta\delta_0}}\right)}{D}\right). \quad \text{(A5)}$$
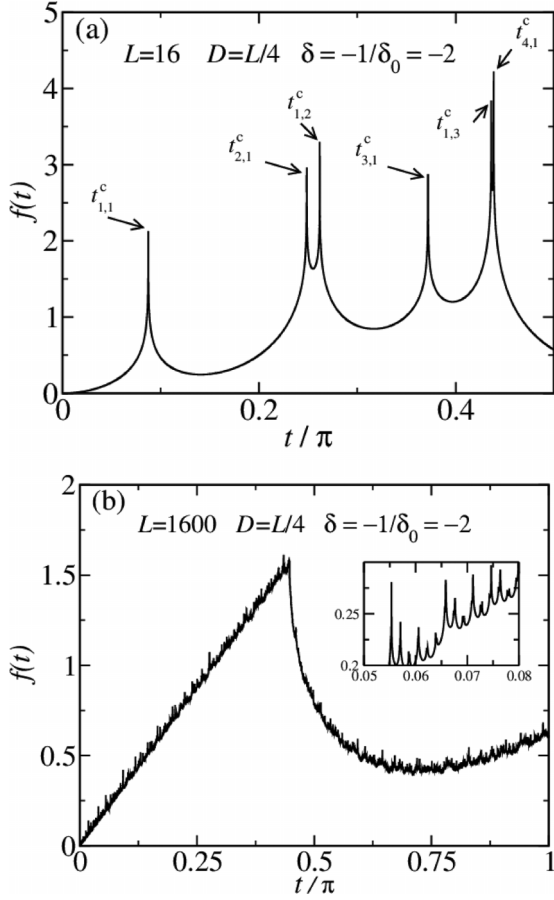
Thus, they vanish $\sim D^{-1}$.

FIG. 6. (a) The dynamic free energy $f(t)$ vs. $t/\pi$ for the case $\nu = 0$, $D = L/4$, $\delta = -\frac{1}{\delta_0} = -2$. (a) For a system size $L = 16$. The arrows indicate the critical time positions given by Eq. (A6). (b) The same as (a) but $L = 1600$. Inset: shows a zoom of the region close to $t = 0.06\pi$.



FIG. 7. (a) The dispersion relation $\pm\omega_{q,\delta}(\nu, D)$ vs. $q$ for systems under PBC and APBC (see legend) with $L = 100$, $\nu = 0$, $\delta = 0.5$, and $D = L/4$. The symbols are the data obtained from Eqs. (A8) and (A11). The solid lines connect the fitted points using Eqs. (A10) and (A12).

#### b. Case $D = L/4$ and $\delta\delta_0 = -1$

When $\delta\delta_0 = -1$, Eq. (A3) becomes $q_k^c = \frac{\pi}{2D}(2k - \frac{3}{2})$. The Fourier wave vectors in (2) are $q_n = \frac{2\pi}{L}(n - \frac{\phi}{2})$. Thus, interestingly, when $D = L/4$ and the antiperiodic boundary condition is considered ($\phi = 1$), all critical wave vectors $q_k^c$ exist even for finite systems (evidently, $L$ is a multiple of 4). The associated critical instants are

$$t_{k,m}^c = (2m - 1)\pi \frac{1}{\sqrt{1 + \delta^2}} \sin\left(q_k^c\right). \quad (A6)$$

Notice also that, because the zeros of $Z$ are on the real-time axis even for finite systems, the dynamic free energy diverges at $t_{m,k}^c$. Similar nonanalyticities at finite systems were observed in other models [13,15,45]. We illustrate this peculiar behavior of the $f(t)$ in Fig. 6 for a quench where $\delta = -\frac{1}{\delta_0} = 2$ and $L = 16$ and $L = 1600$. The peaks are finite due to the finite time step we used ($\sim 10^{-4}$). Evidently, $f(t)$ becomes analytic in the thermodynamic limit as there will be a continuous distribution of YLF zeros over the real-time axis.
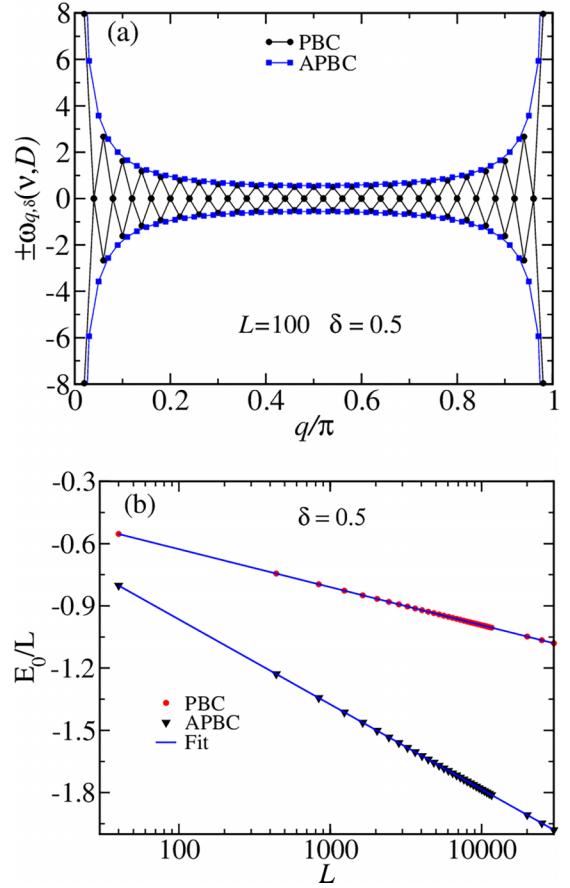
#### 2. Ground-state energy for $D = L/4$

We now compute the ground-state energy for systems with PBC ($\phi = 0$) and APBC ($\phi = 1$), $\nu = 0$, and $D = L/4$. The dispersion (6) becomes

$$\omega_{q_n,\delta} = \frac{\sqrt{\phi + \delta^2(1 + 2(1 - \phi)(-1)^n)^2}}{2 \sin q_n}, \quad (A7)$$

for $n = 1, \ldots, \frac{L}{2}$, except for $n = \frac{L}{2}$ and $\phi = 0$. Instead, in that case, $\omega_{\pi,\delta} = \frac{L}{4}$. Notice that the system is gapless (gapful) for PBC (APBC) $\phi = 0$ ($\phi = 1$) regardless of the value of the dimerization parameter $\delta$. A similar situation appears in the topological insulators (TIs). However, in the TIs the bulk is gapped under PBC and there are gapless boundary states for OBC. In the present model, we have gapless states in the bulk for the PBC case, and a gapped state for $\phi \neq 0$. In Fig. 7(a), we illustrate the dispersion relation Eq. (25) for $L = 100$ and $\delta = 0.5$ for the model with PBC and APBC. It is interesting to note that, in the thermodynamic limit, the system with PBC has two degenerate flat bands.

The ground-state energy $E_0^{\text{APBC}}(\delta, \nu = 0)$ for the system with APBC is

$$E_0^{\text{APBC}}(\delta, 0) = -\frac{\sqrt{1 + \delta^2}}{2} \sum_{n=1}^{\frac{L}{2}} \frac{1}{\sin q_n}. \quad \text{(A8)}$$

We can replace a sum by a integral by using the Euler-Maclaurin sum

$$\sum_{m=0}^{n} F(a + kh) = \frac{1}{h} \int_a^b F(q)dq + \frac{1}{2}[F(b) + F(a)] + R, \quad \text{(A9)}$$

where $R$ is the residual term. So,

$$E_0^{\text{APBC}}(\delta, 0) = -L \frac{\sqrt{1 + \delta^2}}{4\pi} \left\{ \int_{\pi/L}^{\pi - \pi/L} \frac{dq}{\sin q} + \frac{2\pi}{L \sin(\pi/L)} \right.$$
$$\left. + \frac{2\pi R}{L} \right\},$$
$$= -L \frac{\sqrt{1 + \delta^2}}{2\pi} \left\{ \ln\left[\frac{\cos(\pi/2L)}{\sin(\pi/2L)}\right] + \frac{\pi}{L \sin(\pi/L)} \right.$$
$$\left. + \pi a_1 \right\}, \quad \text{(A10)}$$

where we use the fact that the residual term $R = La_1$. We were not able to obtain the exact value of $a_1$. However, we

obtain that $a_1 = 0.08596$ by fitting the exact data Eq. (A8) with Eq. (A10) [see Fig. 7(b)]. We verify that $a_1$ does not depend on $\delta$. For large values of $L$, the energy per site becomes $E_0^{\text{APBC}}(\delta, 0)/L = -\frac{\sqrt{1+\delta^2}}{2\pi}[\ln(2L/\pi) + 2 + \pi a_1]$. Note that the energy is not extensive. However, we can recover the extensivity if we consider the volume of the system as $V = L \ln L$.

For periodic boundary conditions, the ground-state energy for $L$ multiple of 4 is

$$E_0^{\text{PBC}}(\delta, 0) = -\frac{L}{4} - |\delta| \sum_{m=0}^{\frac{L}{4}-1} \frac{1}{\sin[2\pi/L(2m+1)]}. \quad \text{(A11)}$$

Similarly as the APBC case, we obtain

$$E_0^{\text{PBC}}(\delta, 0) = -\frac{L}{4} - L\frac{|\delta|}{2\pi} \left\{ \ln\left[\frac{\cos(\pi/L)}{\sin(\pi/L)}\right] + \frac{2\pi}{L \sin(2\pi/L)} \right.$$
$$\left. + 2\pi a_2 \right\}, \quad \text{(A12)}$$

where $a_2 = 0.04297 \approx a_1/2$ as expected since the residual term depends on the interval and on $h$, which are basically the same in the thermodynamic limit. In this case, for large values of $L$, the energy per site becomes $E_0^{\text{PBC}}(\delta, 0)/L = -\frac{1}{4} - \frac{|\delta|}{2\pi}[\ln(L/\pi) + 2 + 2\pi a_2]$. Note that $E_0^{\text{APBC}} - E_0^{\text{PBC}} \sim -(\sqrt{1 + \delta^2} - |\delta|)L \ln(L)$.

[1] S. Sachdev, *Quantum Phase Transitions*, 2nd ed. (Cambridge University Press, Cambridge, 2011).

[2] H. E. Stanley, *Introduction to Phase Transitions and Critical Phenomena* (Oxford University Press, Oxford, 1987).

[3] S. L. Sondhi, S. M. Girvin, J. P. Carini, and D. Shahar, Continuous quantum phase transitions, Rev. Mod. Phys. **69**, 315 (1997).

[4] C. N. Yang and T. D. Lee, Statistical theory of equations of state and phase transitions. I. Theory of condensation, Phys. Rev. **87**, 404 (1952).

[5] T. D. Lee and C. N. Yang, Statistical theory of equations of state and phase transitions. II. Lattice gas and ising model, Phys. Rev. **87**, 410 (1952).

[6] M. E. Fisher, *The Nature of Critical Points*, Lectures in Theoretical Physics Vol. viic, edited by W. E. Brittin (Golden and Breach, New York, 1965).

[7] B.-B. Wei and R.-B. Liu, Lee-yang zeros and critical times in decoherence of a probe spin coupled to a bath, Phys. Rev. Lett. **109**, 185701 (2012).

[8] X. Peng, H. Zhou, B.-B. Wei, J. Cui, J. Du, and R.-B. Liu, Experimental observation of lee-yang zeros, Phys. Rev. Lett. **114**, 010601 (2015).

[9] J. L. Cardy, Boundary conditions, fusion rules and the Verlinde formula, Nucl. Phys. B **324**, 581 (1989).

[10] J. L. Cardy and D. C. Lewellen, Bulk and boundary operators in conformal field theory, Phys. Lett. B **259**, 274 (1991).

[11] A. LeClair, G. Mussardo, H. Saleur, and S. Skorik, Boundary energy and boundary states in integrable quantum field theories, Nucl. Phys. B **453**, 581 (1995).

[12] M. Heyl, A. Polkovnikov, and S. Kehrein, Dynamical quantum phase transitions in the transverse-field ising model, Phys. Rev. Lett. **110**, 135704 (2013).

[13] F. Andraschko and J. Sirker, Dynamical quantum phase transitions and the loschmidt echo: A transfer matrix approach, Phys. Rev. B **89**, 125120 (2014).

[14] S. Vajna and B. Dóra, Disentangling dynamical phase transitions from equilibrium phase transitions, Phys. Rev. B **89**, 161105(R) (2014).

[15] C. Karrasch and D. Schuricht, Dynamical phase transitions after quenches in nonintegrable models, Phys. Rev. B **87**, 195104 (2013).

[16] E. Canovi, P. Werner, and M. Eckstein, First-order dynamical phase transitions, Phys. Rev. Lett. **113**, 265702 (2014).

[17] S. Vajna and B. Dóra, Topological classification of dynamical phase transitions, Phys. Rev. B **91**, 155127 (2015).

[18] J. C. Halimeh and V. Zauner-Stauber, Dynamical phase diagram of quantum spin chains with long-range interactions, Phys. Rev. B **96**, 134427 (2017).

[19] B. Žunkovič, M. Heyl, M. Knap, and A. Silva, Dynamical quantum phase transitions in spin chains with long-range interactions: Merging different concepts of nonequilibrium criticality, Phys. Rev. Lett. **120**, 130601 (2018).

[20] N. Fläschner, D. Vogel, M. Tarnowski, B. S. Rem, D.-S. Lühmann, J. C. Budich, L. Mathey, K. Sengstock, and C. Weitenberg, Quasiparticle engineering and entanglement propagation in a quantum many-body system, Nature Phys. **14**, 265 (2018).

[21] R. Jafari, H. Johannesson, A. Langari, and M. A. Martin-Delgado, Quench dynamics and zero-energy modes: The case of the creutz model, Phys. Rev. B **99**, 054302 (2019).

[22] R. Jafari, Dynamical quantum phase transition and quasi particle excitation, Sci. Rep. **9**, 2871 (2019).

[23] X.-Y. Guo, C. Yang, Y. Zeng, Y. Peng, H.-K. Li, H. Deng, Y.-R. Jin, S. Chen, D. Zheng, and H. Fan, Observation of a dynamical quantum phase transition by a superconducting qubit simulation, Phys. Rev. Appl. **11**, 044080 (2019).

[24] V. Zauner-Stauber and J. C. Halimeh, Probing the anomalous dynamical phase in long-range quantum spin chains through fisher-zero lines, Phys. Rev. E **96**, 062118 (2017).

[25] P. Jurcevic, H. Shen, P. Hauke, C. Maier, T. Brydges, C. Hempel, B. P. Lanyon, M. Heyl, R. Blatt, and C. F. Roos, Direct observation of dynamical quantum phase transitions in an interacting many-body system, Phys. Rev. Lett. **119**, 080501 (2017).

[26] I. Homrighausen, N. O. Abeling, V. Zauner-Stauber, and J. C. Halimeh, Anomalous dynamical phase in quantum spin chains with long-range interactions, Phys. Rev. B **96**, 104436(R) (2017).

[27] J. A. Hoyos, R. F. P. Costa, and J. C. Xavier, Disorder-induced dynamical griffiths singularities after certain quantum quenches, Phys. Rev. B **106**, L140201 (2022).

[28] M. Heyl, Dynamical quantum phase transitions: A review, Rep. Prog. Phys. **81**, 054001 (2018).

[29] R. Islam, C. Senko, W. C. Campbell, S. Korenblit, J. Smith, A. Lee, E. E. Edwards, C.-C. J. Wang, J. K. Freericks, and C. Monroe, Emergence and frustration of magnetism with variable-range interactions in a quantum simulator, Science **340**, 583 (2013).

[30] D. Porras and J. I. Cirac, Effective quantum spin systems with trapped ions, Phys. Rev. Lett. **92**, 207901 (2004).

[31] C. Monroe, W. C. Campbell, L.-M. Duan, Z.-X. Gong, A. V. Gorshkov, P. W. Hess, R. Islam, K. Kim, N. M. Linke, G. Pagano, P. Richerme, C. Senko, and N. Y. Yao, Programmable quantum simulations of spin systems with trapped ions, Rev. Mod. Phys. **93**, 025001 (2021).

[32] J. Marino, M. Eckstein, M. S. Foster, and A. M. Rey, Dynamical phase transitions in the collisionless pre-thermal states of isolated quantum systems: Theory and experiments, Rep. Prog. Phys. **85**, 116001 (2022).

[33] J. Zhang, G. Pagano, P. W. Hess, A. Kyprianidis, P. Becker, H. Kaplan, A. V. Gorshkov, Z.-X. Gong, and C. Monroe, Observation of a many-body dynamical phase transition with a 53-qubit quantum simulator, Nature (London) **551**, 601 (2017).

[34] M. K. Joshi, A. Schuckert, I. Lovas, C. Maier, R. Blatt, and C. F. Knap, Roos, Observing emergent hydrodynamics

[35] B. Žunkovič, A. Silva, and M. Fabrizio, Dynamical phase transitions and loschmidt echo in the infinite-range XY model, Phil. Trans. R. Soc. A **374**, 20150160 (2016).

[36] A. Kosior and K. Sacha, Dynamical quantum phase transitions in discrete time crystals, Phys. Rev. A **97**, 053621 (2018).

[37] M. Suzuki, The dimer problem and the generalized *X*-model, Phys. Lett. A **34**, 338 (1971).

[38] D. Eloy and J. C. Xavier, Entanglement entropy of the low-lying excited states and critical properties of an exactly solvable two-leg spin ladder with three-spin interactions, Phys. Rev. B **86**, 064421 (2012).

[39] N. G. Jones, Symmetry-resolved entanglement entropy in critical free-fermion chains, J. Stat. Phys. **188**, 28 (2022).

[40] A. Dutta and A. Dutta, Probing the role of long-range interactions in the dynamics of a long-range Kitaev chain, Phys. Rev. B **96**, 125113 (2017).

[41] N. Defenu, T. Enss, and J. C. Halimeh, Dynamical criticality and domain-wall coupling in long-range hamiltonians, Phys. Rev. B **100**, 014434 (2019).

[42] P. Uhrich, N. Defenu, R. Jafari, and J. C. Halimeh, Out-of-equilibrium phase diagram of long-range superconductors, Phys. Rev. B **101**, 245148 (2020).

[43] W. P. Su, J. R. Schrieffer, and A. J. Heeger, Solitons in polyacetylene, Phys. Rev. Lett. **42**, 1698 (1979).

[44] F. Ares, S. Murciano, and P. Calabrese, Symmetry-resolved entanglement in a long-range free-fermion chain, J. Stat. Mech.: Theory Exp. (2022) 063104.

[45] J. A. Hoyos, J. C. Xavier, and R. F. P. Costa, Dynamical Griffiths singularities in certain random spin chains (unpublished).

[46] G. Jaeger, Classification of phase transitions: Introduction and evolution, Arch. Hist. Exact Sci. **53**, 51 (1998).

[47] M. Schmitt and S. Kehrein, Dynamical quantum phase transitions in the Kitaev honeycomb model, Phys. Rev. B **92**, 075114 (2015).

[48] N. Byers and C. N. Yang, Theoretical considerations concerning quantized magnetic flux in superconducting cylinders, Phys. Rev. Lett. **7**, 46 (1961).

[49] W. Kohn, Theory of the insulating state, Phys. Rev. **133**, A171 (1964).

[50] D. Poilblanc, Twisted boundary conditions in cluster calculations of the optical conductivity in two-dimensional lattice models, Phys. Rev. B **44**, 9562 (1991).

in a long-range quantum magnet, Science **376**, 720 (2022).